Acta Biomaterialia 6 (2010) 1661–1670

Contents lists available at ScienceDirect

Acta Biomaterialia

journal homepage: www.elsevier.com/locate/actabiomat

Effects of phosphoric acid treatment of titanium surfaces on surface properties, osteoblast response and removal of torque forces

Jin-Woo Park [a,b,*], Youn-Jeong Kim [b], Je-Hee Jang [b], Tae-Geon Kwon [c], Yong-Chul Bae [d], Jo-Young Suh [a]

[a] Department of Periodontology, School of Dentistry, Kyungpook National University, 188-1, Samduk 2Ga, Jung-Gu, Daegu 700-412, Republic of Korea
[b] Bio-implant Interface Research Laboratory, School of Dentistry, Kyungpook National University, 188-1, Samduk 2Ga, Jung-Gu, Daegu 700-412, Republic of Korea
[c] Department of Oral & Maxillofacial Surgery, School of Dentistry, Kyungpook National University, 188-1, Samduk 2Ga, Jung-Gu, Daegu 700-412, Republic of Korea
[d] Department of Oral Anatomy & Neurobiology, School of Dentistry, Kyungpook National University, 188-1, Samduk 2Ga, Jung-Gu, Daegu 700-412, Republic of Korea

ARTICLE INFO

Article history:
Received 17 July 2009
Received in revised form 29 September 2009
Accepted 5 October 2009
Available online 9 October 2009

Keywords:
Titanium implant
Osteoblast differentiation
Phosphate chemistry
Surface wettability
Osseointegration

ABSTRACT

This study investigated the surface characteristics and biocompatibility of phosphate ion (P)-incorporated titanium (Ti) surfaces hydrothermally treated with various concentrations of phosphoric acid (H_3PO_4). The surface characteristics were evaluated by scanning electron microscopy, thin-film X-ray diffractometry, X-ray photoelectron spectroscopy, optical profilometry, contact angle and surface energy measurement and inductively coupled plasma mass spectroscopy (ICP-MS). MC3T3-E1 cell attachment, spreading, proliferation and osteoblastic gene expression on different surfaces were evaluated. The degree of bony integration was biomechanically evaluated by removal torque testing after 4 weeks of healing in rabbit tibiae. The H_3PO_4 treatment produced micro-rough Ti surfaces with crystalline P-incorporated Ti oxide layers. High concentration H_3PO_4 treatment (1% and 2%) produced significantly higher hydrophilic surfaces compared with low H_3PO_4 treatment (0.5%) and untreated surfaces ($P < 0.01$). ICP-MS analysis showed P ions were released from P-incorporated surfaces. Significant increased cell attachment ($P < 0.05$) and notably higher mRNA expressions of Runx2, alkaline phosphatase, osteopontin and osteocalcin were observed in cells grown on P-incorporated surfaces compared with cells on untreated machined surfaces. P-incorporated surfaces showed significantly higher removal torque forces compared with untreated machined implants ($P < 0.05$). Ti surfaces treated with 2% H_3PO_4 showed increasing tendencies in osteoblastic gene expression and removal torque forces compared with those treated with lower H_3PO_4 concentrations or untreated surfaces. These results demonstrate that H_3PO_4 treatment may improve the biocompatibility of Ti implants by enhancing osteoblast attachment, differentiation and biomechanical anchorage.

1. Introduction

Numerous studies have demonstrated that a titanium (Ti) oxide layer modified by various methods improves bone healing around Ti implants. A micro-porous crystalline Ti oxide layer or one incorporated with potentially bioactive ions accelerates implant bone healing by promoting osteoblast cell differentiation in vitro, and by increasing bone–implant contact and biomechanical anchorage in vivo [1–6].

Several studies have performed anodic oxidation treatment using phosphoric acid in order to produce biocompatible Ti surfaces for biomedical applications [5,7,8]. These, however, did not produce crystalline phosphate ion (P)-incorporated oxide layers. Recently, we have shown that hydrothermal treatment using phosphoric acid produces a crystalline P-incorporated oxide surface, which exhibited highly wettable and micro-rough surface features [9]. P-incorporated Ti surfaces significantly increased bone–implant contact percentages and removal torque forces in rabbittibiae compared with various commercial microstructured surfaces.

Surface properties, including micro-topography, chemistry and wettability, are important factors affecting the quality of bone healing by influencing the biological responses of bone-interfacing implants [1–6,9–14]. Thus, Ti implants with surface properties that combine optimal micro-roughness, superior wettability and potentially bioactive chemistry may be effective for achieving favorable implant bone healing. Micro-rough P-incorporated surfaces showed improved osseointegration in vivo [9], but it might be expected that P-incorporated oxide layers produced by various hydrothermal treatment conditions would have different surface properties, which may affect their osteoconductivity.

* Corresponding author. Address: Department of Periodontology, School of Dentistry, Kyungpook National University, 188-1, Samduk 2Ga, Jung-Gu, Daegu 700-412, Republic of Korea. Tel.: +82 53 600 7523; fax: +82 53 257 6883.
E-mail addresses: jinwoo@knu.ac.kr, jw94821@hanafos.com (J.-W. Park).

1742-7061/$ - see front matter © 2009 Acta Materialia Inc. Published by Elsevier Ltd. All rights reserved.
doi:10.1016/j.actbio.2009.10.011

Table 1
Primer sequences for polymerase chain reaction.

Target	Primer sequences
Runx2	Forward primer 5′–3′: CCAGAATGATGGTGTTGACG Reverse primer 5′–3′: GGTTGCAAGATCATGACTAGGG
ALP	Forward primer 5′–3′: CTTGACTGTGGTTACTGCTG Reverse primer 5′–3′: GAGCGTAATCTACCATGGAG
Osteopontin	Forward primer 5′–3′: TCAAGTCAGCTGGATGAACC Reverse primer 5′–3′: CTTGTCCTTGTGGCTGTGAA
Osteocalcin	Forward primer 5′–3′: TGCTTGTGACGAGGTATCAG Reverse primer 5′–3′: GTGACATCCATACTTGCAGG
GAPDH	Forward primer 5′–3′: GGCATTGCTCTCAATGACAA Reverse primer 5′–3′: TGTGAGGGAGATGCTCAGTG

GAPDH: glyceraldehydes-3-phosphate dehydrogenase.

Therefore, the aim of this study was to investigate the surface characteristics of Ti surfaces produced by varying the phosphoric acid concentrations for use in future biomedical applications. The surface in vitro osteoconductivity was evaluated by observing cell attachment, spreading, proliferation and osteoblastic gene expression using MC3T3-E1 pre-osteoblast cells, and in vivo implant integration was biomechanically evaluated by comparing removal torque forces in rabbit tibiae.

2. Materials and methods

2.1. Sample preparation

Disks made from commercially pure Ti (ASTM grade 3) rods, 14 mm in diameter and 2 mm thick, were used to characterize

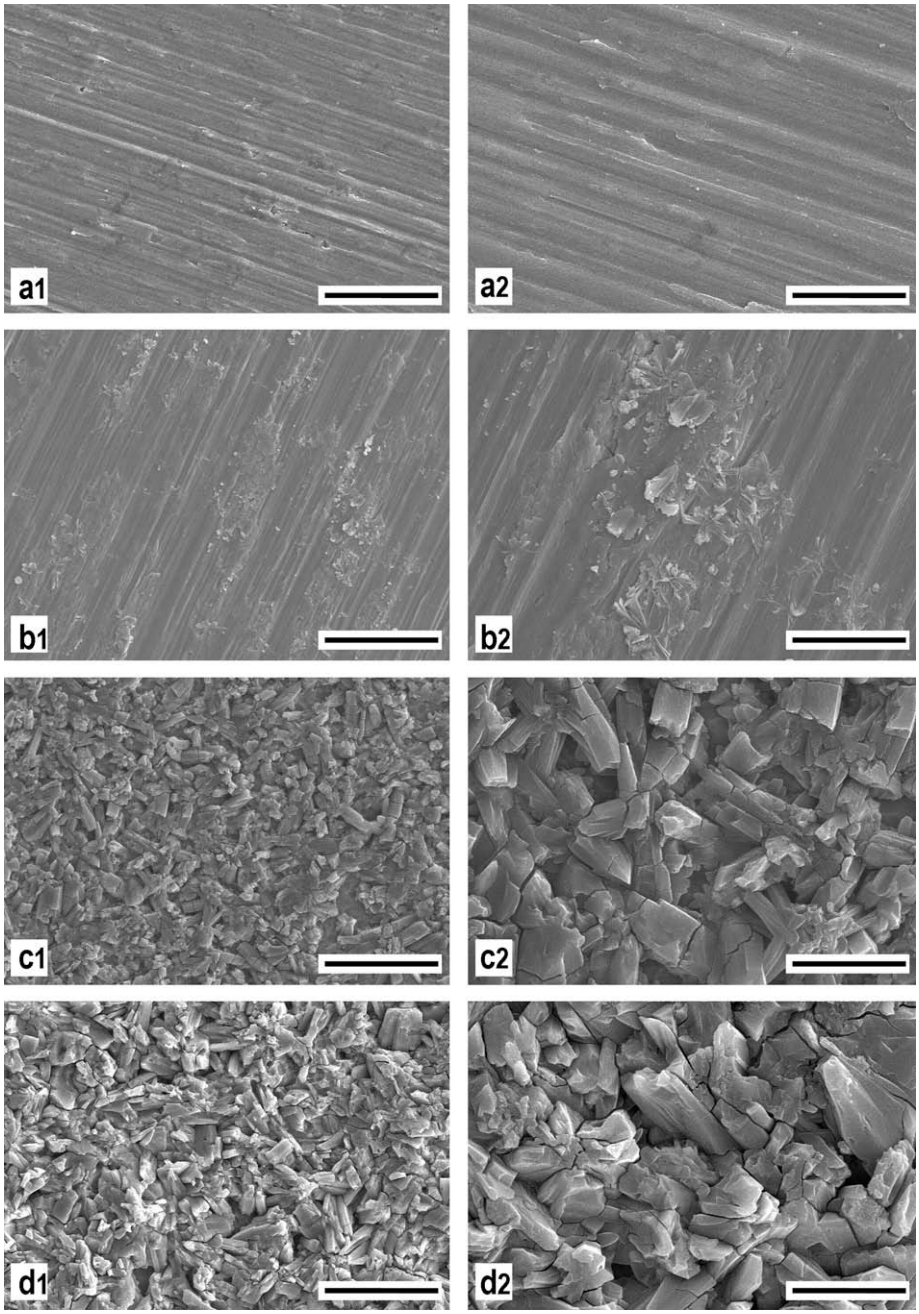

Fig. 1. Scanning electron microscope images of different samples. (a1 and a2) machined, (b1 and b2) TiP-1, (c1 and c2) TiP-2 and (d1 and d2) TiP-3 surfaces at magnifications of 1000× (a1–d1) and 3000× (a2–d2). SEM images show different surface morphologies of investigated samples. Scale bars = 30 μm (a1–d1) and 10 μm (a2–d2).

the surface properties and for cell culture experiments. To prepare the Ti disks with a surface structure similar to that of commercial machine-turned implants, they were wet-abraded to 1200 grit SiC abrasive paper and successively cleaned in acetone, alcohol and deionized water (machined surface). To produce various P-incorporated Ti oxide surfaces, the machine-surfaced Ti disks were treated hydrothermally using 0.5% (TiP-1), 1% (TiP-2) and 2% (TiP-3) (w/w) H_3PO_4 solutions at 180 °C for 2 h in a Teflon-lined reactor, followed by heat treatment according to methods described previously [9,15] Four different Ti surfaces were used: (1) machined surface, (2) TiP-1 surface, (3) TiP-2 surface and (4) TiP-3 surface. For the animal study, screw-type implants ($n = 28$), with an external diameter of 3.3 mm and a length of 5.3 mm, were prepared from commercially pure Ti (ASTM grade 3) rods. The screw implants were turned and then further treated with the same methods used to produce the P-incorporated Ti disks. All samples were sterilized by γ-irradiation before the cell culture and animal experiments.

2.2. Surface characterization

The surface morphologies of the samples were observed by scanning electron microscopy (SEM; S-4300, Hitachi, Tokyo, Japan). The crystalline structure and chemical composition of the oxide layer were investigated by thin-film X-ray diffractometry (XRD; X'Pert-APD, Philips, Almelo, The Netherlands) and X-ray photoelectron spectroscopy (XPS; Quantera SXM, ULVAC-PHI, Tokyo, Japan). After acquiring XPS data, samples were cleaned with argon sputtering for 30 s in order to remove surface contaminants, and then chemical composition, binding energies and peak areas were further measured. Surface roughness measurements of the disks were taken with optical profilometry (WYKO NT 2000, Veeco Instruments Inc., Woodbury, NY, USA) over a 320 × 240 μm area. Three disks from each group were measured and two measurements were performed on each disk. The thickness of the P-incorporated Ti oxide layer was evaluated by SEM measurements using cross-sectioned samples. Surface wettabilities of the different surfaces were determined by measuring the contact angles with one drop (5 μl) of deionized water using an automatic contact angle meter (Phoenix 300; Surface Electro Optics, Seoul, Korea). Three samples from each group were measured and two measurements were performed on each sample to evaluate the average contact angle at 10 s.

For ionic release measurement, three disks of each group were immersed in 20 ml of physiological saline solution (0.9% NaCl) in a sealed bottle at 37 °C for 1, 3 and 7 days with gentle shaking. After immersion, the concentration of phosphorus ions released from the samples into the solution was measured by inductively coupled plasma mass spectroscopy (ICP-MS; ELAN DRC-e, Perkin-Elmer, Norwalk, CT, USA) at a detection limit of 0.1 ppb. Measurements were repeated three times for each immersion time point.

2.3. Cell culture

MC3T3-E1 cells, a mouse calvaria-derived osteoblast-like cell line, were plated in Dulbecco's modified Eagle's medium (Gibco–BRL Life Technologies, Grand Island, NY, USA) containing 10% fetal bovine serum (Gibco–BRL Life Technologies), 500 U ml^{-1} penicillin (Keunhwa Pharmaceutical, Seoul, Korea), and 500 U ml^{-1} streptomycin (Donga Pharmaceutical, Seoul, Korea). The cells were cultured under 100% humidity and 5% CO_2, at 37 °C. The medium was changed every other day prior to confluence and cells were passaged using 0.05% trypsin/0.02% EDTA.

2.4. Morphological evaluation of early cell spreading using SEM

The cells were seeded on disks in 24-well culture plates at a density of 4×10^4 cells $well^{-1}$. After 1 h of culture, cells attached to the disks were sequentially fixed with 2% glutaraldehyde and 1% osmium tetroxide and dehydrated using an ascending series of alcohols. After critical point drying and gold–palladium coating, the morphologies of the cells on the various Ti surfaces were observed using SEM.

2.5. Initial cell attachment and cell proliferation

For the evaluation of initial cell attachment and proliferation, cells were cultured on Ti disks in 24-well culture plates at an initial seeding density of 4×10^4 cells $well^{-1}$. Initial cell attachment was evaluated after 1 h of culture. For cellular proliferation assay, cells were cultured for 1 and 3 days. Cell attachment and proliferation were assessed by a colorimetric assay based on the conversion of a (2-(2-methoxy-4-nitrophenyl)-3-(4-nitrophenyl)-5-(2,4-disulfophenyl)-2H-tetrazolium, monosodium salt (WST-8)) into the highly water-soluble formazan, enabling assessment of the number of viable cells [16], which were evaluated by using a cell counting kit (CCK-8; Dojindo Molecular Technologies, Tokyo, Japan) in

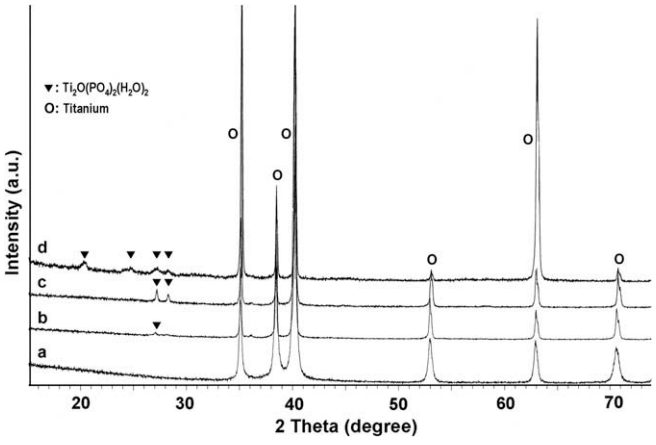

Fig. 2. X-ray diffraction patterns of machined (a), TiP-1 (b), TiP-2 (c) and TiP-3 (d) samples.

Table 2
Surface roughness parameters of machined, TiP-1, TiP-2 and TiP-3 samples ($n = 6$).

Group	R_a (μm)	R_q (μm)	R_t (μm)	S_{dr}
Machined	0.31 ± 0.02	0.39 ± 0.02	3.46 ± 0.52	1.08 ± 0.01
TiP-1	0.32 ± 0.03	0.40 ± 0.04	3.83 ± 0.57	1.15 ± 0.02
TiP-2	0.98 ± 0.03	1.22 ± 0.03	11.92 ± 1.15	1.65 ± 0.03
TiP-3	1.17 ± 0.08	1.56 ± 0.10	14.87 ± 1.50	2.57 ± 0.17

R_a = The arithmetic average of the absolute height values of the profile; R_q = the root mean square of the values of the profile; R_t = the maximum peak-to-valley height of the entire measurement area; S_{dr} = the developed surface area ratio (the ratio of the measured surface area over the sampling area).

Table 3
Chemical composition of investigated surfaces by X-ray photoelectron spectroscopy (at.%).

Group	Ti	O	P	C	N	Ar	Ti/P ratio
Machined	18.8	56.5		24.1	0.6		
Machined[a]	42.6	54.8		<0.1	0.4	2.1	
TiP-1[a]	28.4	66.5	3.0	<0.1	0.2	1.8	9.46
TiP-2[a]	18.3	66.9	13.1	<0.1	0.2	1.4	1.40
TiP-3[a]	15.3	68.6	14.5	<0.1	0.3	1.2	1.05

[a] Ti surface after argon sputter cleaning.

accordance with the manufacturer's instructions. After the indicated incubation times, disks were washed with phosphate buffered saline and transferred to new 24-well plates. A CCK-8 mixture solution prewarmed to 37 °C was added to each well containing a disk and incubated for 3 h. Then, 150 μl of solution was transferred to new 96-well plates and the absorbance was measured at a wavelength of 450 nm using an ELISA microplate reader. The resulting absorbance for each of the wells was averaged and corresponded to the cell numbers with a standard calibration curve prepared using the data obtained from the wells that contain known numbers of viable cells.

2.6. Real-time polymerase chain reaction (PCR)

The cells were seeded on disks in 24-well culture plates at an initial seeding density of 4×10^4 cells well^{-1}, and cultured for 7 and 14 days. Total RNA was extracted from the cultured cells using Trizol reagent (Gibco–BRL Life Technologies) and quantified. To create first-strand cDNAs, reverse transcription was performed as described previously [4]. To determine the Runx2, alkaline phosphatase (ALP), osteopontin, osteocalcin and glyceraldehyde-3-phosphate dehydrogenase mRNA levels, real-time PCR reactions were performed as described previously using the primers shown in Table 1 [4]. The results were expressed as fold differences of gene expression relative to the results of the machined surface at 7 days of culture. All measurements were run in triplicate.

2.7. Animals and surgical procedure

Seven adult male New Zealand White rabbits weighing 3.5–4 kg were used in this study. This experiment was approved by the Institutional Animal Care and Use Committee of Kyungpook National University Hospital, Daegu, Korea. Korean national regulations (equivalent to NIH guidelines; NIH Publication No. 85-23 Rev. 1985) for the care and use of laboratory animals were observed. General anesthesia was induced by intramuscular injection of a combination of 1.3 ml of ketamine (100 mg ml^{-1}; Ketara, Yuhan, Seoul, Korea) and 0.2 ml of xylazine (7 mg kg^{-1} body weight; Rompun, Bayer Korea, Seoul, Korea). The medial surfaces of the proximal tibiae were used as the surgical sites. The surgical areas were

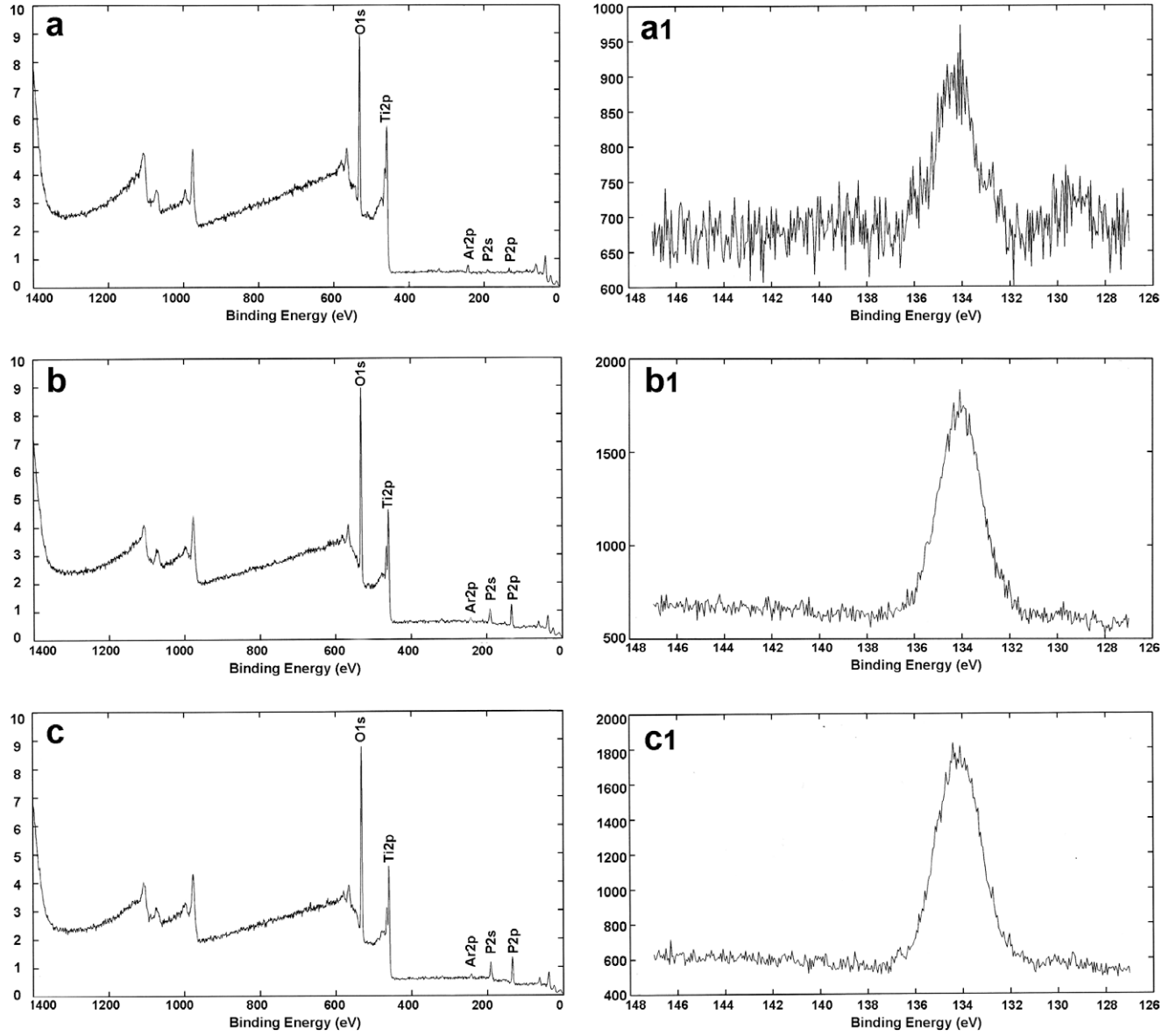

Fig. 3. X-ray photoelectron survey spectra (a–c) and high-resolution P2p spectra (a1–c1) of TiP-1 (a and a1), TiP-2 (b and b1) and TiP-3 (c and c1) surfaces after argon sputter cleaning.

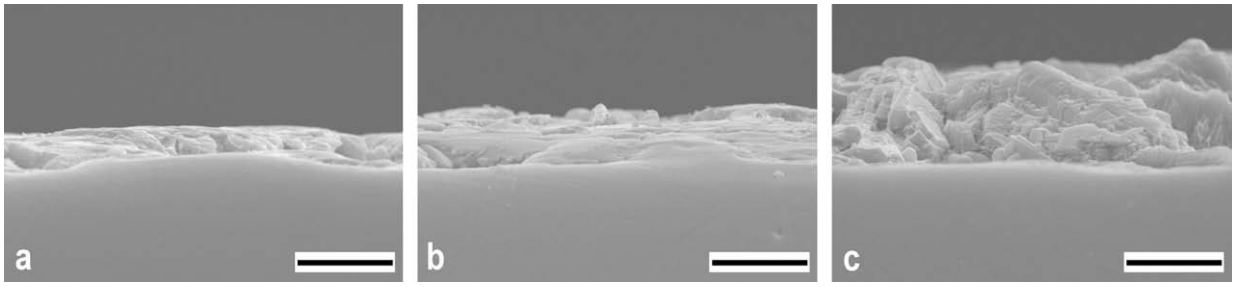

Fig. 4. Scanning electron microscope images of cross-sectioned surfaces showing the thickness of oxide layer of TiP-1 (a), TiP-2 (b) and TiP-3 (c) samples. Scale bar = 5 μm.

shaved and the skin was washed with a mixture of iodine and 70% ethanol before surgical draping. Local anesthesia was induced with 1 ml of 2% lidocaine (1:100,000 epinephrine; Yuhan) to control bleeding and to provide additional local anesthesia. The surgical sites were exposed with an incision through the skin, fascia and periosteum at the medial surface of the proximal tibiae using a sterile surgical technique.

The implant site osteotomies were prepared in the usual manner. A final drill diameter of 2.85 mm was used. All drilling procedures were carried out under profuse sterile saline irrigation. Four different screw-shaped implants were placed in each animal and randomly placed in the right and left tibiae. One tibia received two implants. Screw implants (n = 7 per each group) were inserted with self-tapping and all implants penetrated the first bone cortex only. All implants were placed in their final position with similar insertion torques (20–25 N cm). After surgery, the surgical sites were closed in layers and sutured using Vicryl (Ethicon, Somerville, NJ, USA). Antibiotics (Baytril, Bayer Korea) and analgesics (Nobin, Bayer Korea) were injected intramuscularly for 3 days to prevent postsurgical infection and to control pain. After 4 weeks, the animals were killed by intravenous injections of air under general anesthesia. Tissues were taken for removal torque tests.

2.8. Removal torque tests

Removal torque tests were performed to evaluate implant stability in the bone bed. The removal torque value in Newton centimeters (N cm) reflects the interfacial shear strength [17]. The degree of biomechanical anchorage evaluated by removal torque testing represents the strength of implant integration in bone tissue [18–20]. The tibiae containing the implants were removed en bloc. They were firmly stabilized with a locking vice and the peak removal torque force was measured using a digital torque meter (MG series, Mark-10 Corporation, New York, NY, USA) with a measuring range of 0–135 N cm (7 rabbits; 7 implants per group). A single blinded examiner recorded all measurements of the peak torque to initiate reverse rotation.

2.9. Statistical analysis

Statistical analysis was performed using the SPSS 14 statistical system (SPSS Inc., Chicago, IL, USA). The means and standard deviations of data were calculated. One-way analysis of variance with Tukey's multiple comparisons test was performed to evaluate differences between groups. Values of P less than 0.05 were considered statistically significant.

3. Results

3.1. Surface characteristics

The surface morphologies of the investigated samples are shown in Fig. 1. The machined surface showed typical anisotropic abrasive marks caused by wet abrasion, and H_3PO_4 treatment produced micro-rough surface structures. Low concentrations of H_3PO_4 treatment (0.5% (w/w)) produced a nonhomogenous surface morphology; some micro-rough surface structures were observed sporadically throughout the wet-abraded surface. Micro-rough surface morphologies were more accentuated in the samples treated using high concentrations of H_3PO_4 (2% (w/w)).

Table 2 shows surface roughness parameters of investigated samples. The TiP-3 surface showed the highest R_a values (1.17 μm) followed by TiP-2 (0.98 μm). The TiP-1 (0.32 μm) and machined (0.31 μm) surfaces had almost identical R_a values. 2% (w/w) H_3PO_4 treatment developed the largest surface area. Among the investigated groups, the TiP-3 had the highest surface area ratio (S_{dr}) value (2.57), and the machined surface (1.08) had the lowest.

Fig. 2 shows XRD patterns of investigated samples. The machined surface was composed of Ti peaks. H_3PO_4 treatment and post-heat treatment produced crystalline titanium oxide phosphate hydrate ($(Ti_2O(PO_4)_2(H_2O)_2$, Joint Committee on Powder Diffraction Standards #88-0041) surface layers. More $Ti_2O(PO_4)_2(H_2O)_2$ peaks were observed in the samples with an increased concentration of H_3PO_4.

Table 3 shows the chemical compositions of the investigated samples determined by XPS analysis. The surfaces of the machined sample primary consisted of Ti and oxygen (O); carbon

Table 4
Contact angle of machined, TiP-1, TiP-2 and TiP-3 samples (mean ± SD; n = 6).

Group	Contact angle (°)
Machined	54.3 ± 2.7[A]
TiP-1	42.9 ± 4.4[B]
TiP-2	11.7 ± 2.6[C]
TiP-3	8.9 ± 3.1[C]
P-value[*]	<0.01

[A–C] The same letters indicate that the values are not significantly different by Tukey's multiple comparison at α = 0.05.
[*] P-values are computed by one-way ANOVA.

Table 5
Release of P ions from TiP-1, TiP-2 and TiP-3 samples (mean ± SD; n = 3).

Group	Immersion time (days)	P (ppb)[a]
TiP-1	1	6.3 ± 0.3
	3	38.9 ± 1.5
	7	70.8 ± 1.1
TiP-2	1	61.6 ± 2.9
	3	98.0 ± 0.5
	7	115.6 ± 0.6
TiP-3	1	75.2 ± 3.1
	3	98.8 ± 2.6
	7	197.8 ± 0.6

[a] Concentration of total three disks per group.

(C) and nitrogen (N) were detected as surface contaminants. The surfaces of treated samples consisted of Ti, O and phosphorus (P). After argon sputter cleaning, the atomic percentages of P for TiP-1, TiP-2 and TiP-3 samples were 3.0, 13.1 and 14.5, respectively. Argon was detected as a surface contaminant on sputter-cleaned samples. Fig. 3 shows the XPS survey spectra and high-resolution P2p spectra of the TiP-1, TiP-2 and TiP-3 samples after argon sputter cleaning. Using the charge shift of C1s main peak, the P2p peaks at 133.4 eV for the TiP-1, TiP-2 and TiP-3 samples corresponded to the binding energy of P in PO_4^{3-} [21].

Fig. 4 shows the cross-sectional SEM images of the P-incorporated surfaces. The thickest portion of the area showing plate-like surface structures in the TiP-1 sample (which did not show homogeneous surface coating) was approximately 1.5 μm. The thicknesses of the P-incorporated oxide layers of the TiP-2 and TiP-3 surfaces were approximately 3 and 5 μm, respectively.

The P-incorporated surfaces (TiP-1, TiP-2 and TiP-3) showed significantly lower water contact angles and significantly greater surface energy than the machined surfaces ($P < 0.01$; Table 4). The TiP-2 and TiP-3 surfaces were more hydrophilic than the TiP-1 surface ($P < 0.01$), but there were no significant differences in contact angles or surface energies between the TiP-2 and TiP-3 surfaces.

ICP-MS analysis revealed that P ions were released from the P-incorporated samples into the physiological saline solution (Table 5). The concentrations of the released P ions increased with increasing incubation time. The TiP-2 and TiP-3 samples showed more P ions than the TiP-1 samples.

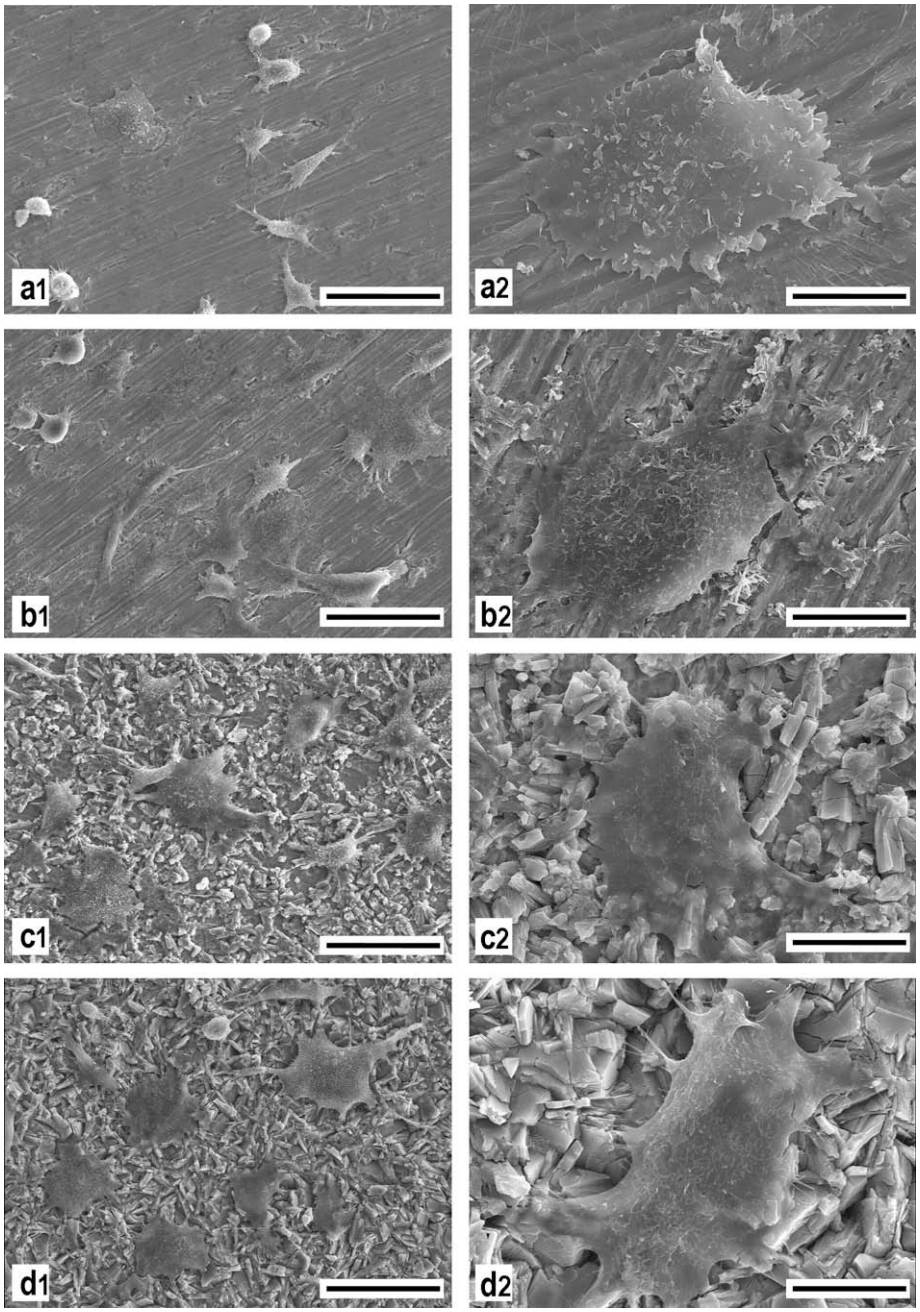

Fig. 5. Scanning electron microscope images showing the morphology of spread cells on machined (a1 and a2), TiP-1 (b1 and b2), TiP-2 (c1 and c2) and TiP-3 (d1 and d2) surfaces after 1 h of incubation at magnifications of 600× (a1–d1), 2000× (b2–d2) and 2500× (a2). Scale bars = 50 μm (a1–d1), 15 μm (b2–d2) and 12 μm (a2).

3.2. Morphological evaluation of spread cells

Fig. 5 shows SEM images of spread cells on different Ti samples at 1 h of incubation. Fully spread cells on machined and TiP-1 surfaces were in very close contact with the underlying surfaces with numerous filopodial attachments, which seems to be attributed to relatively smooth surface features. In contrast, spread cells on micro-rough surfaces (TiP-2 and TiP-3) were attached to the surfaces with gaps between the ventral surfaces of cells and lower surface structures; cells were anchored to protruding surface microstructures by cytoplasmic processes and filopodial attachments. The P-incorporated micro-rough surfaces showed a better spread appearance of cells compared with relatively smooth surfaces.

3.3. Cell attachment and proliferation

After 1 h of culture, there were significantly more attached cells on the P-incorporated surfaces than on the machined surface ($P < 0.05$; Fig. 6). The numbers of proliferated cells on the P-incorporated surfaces showed tendencies to increase compared with the machined surfaces (Fig. 7). At 1 day of culture, the P-incorporated surfaces showed significantly higher cell numbers than the machined surfaces ($P < 0.05$). At 3 days, there were no differences in cell numbers among the investigated groups.

3.4. Osteoblast gene expression

Fig. 8 shows the levels of osteoblastic gene expression. At 7 days, the mRNA levels of Runx2 on TiP-3 (3.0-fold), TiP-2 (2.5-fold) and TiP-1 (1.9-fold) surfaces were markedly higher than on the machined surfaces. At 14 days, the Runx2 expressions were slightly increased or showed similar levels when compared with those at 7 days; Runxs2 expressions were higher on the P-incorporated surfaces than on the machined surfaces. The mRNA expressions of ALP, osteopontin and osteocalcin genes paralleled a similar induction to the Runx2 at 7 and 14 days. Increased Runx2 expressions on the P-incorporated surfaces at 7 days resulted in concomitant increases in osteopontin and osteocalcin expressions on those surfaces at 7 days. Increased Runx2 expressions on the P-incorporated surfaces at 14 days resulted in concomitant increases in ALP and osteocalcin expressions on those surfaces at 14 days. ALP mRNA expression levels were similar between groups at 7 days and increased with incubation time for all groups. At 14 days, the ALP expressions on the P-incorporated surfaces were higher than on the machined surfaces. The mRNA levels of osteopontin were notably higher on the P-incorporated surfaces than on the machined surfaces at 7 days (2.0- to 5.3-fold). At 14 days, the osteopontin mRNA levels then decreased or maintained a level similar to that at 7 days. In all groups, the osteocalcin mRNA expressions at 14 days were greater than at 7 days. The mRNA levels of osteocalcin on the P-incorporated surfaces were higher than on the machined surfaces at 7 days (1.7- to 2.8-fold). At 14 days, the osteocalcin expressions in cells grown on the P-incorporated surfaces were slightly higher than on the machined surfaces. The TiP-3 surface showed higher expressions of Runx2, ALP, osteopontin and osteocalcin compared with the other surfaces. The results of repeated experiments showed similar gene expression patterns.

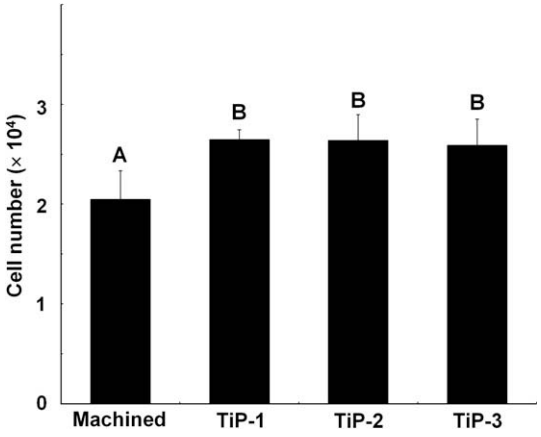

Fig. 6. Number of attached cells on different Ti surfaces at 1 h of culture. Data are presented as the mean ± SD ($n = 7$ per group). [A,B]The same letters are not significant by Tukey's multiple comparison at $\alpha = 0.05$.

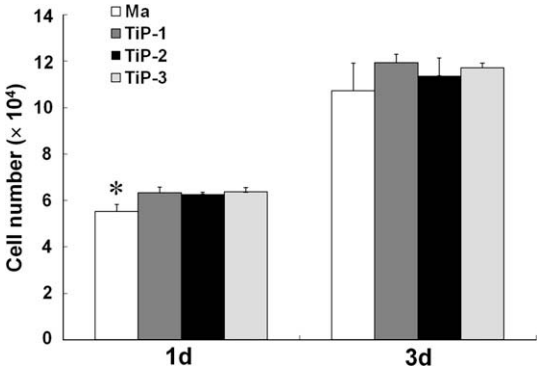

Fig. 7. Number of proliferated cells on the different Ti surfaces after 1 and 3 days of culture. Data are presented as the mean ± SD ($n = 5$ per group). *Statistically significant difference compared to TiP-1, TiP-2 and TiP-3 surfaces ($P < 0.05$).

3.5. Removal torque testing

All the P-incorporated implants showed mean removal torque values (RTV) higher than the machine-turned implants (Fig. 9). The mean RTV of TiP-1 was higher than the machined surface; the difference was marginally significant ($P = 0.053$). The mean RTVs of the TiP-2 and TiP-3 implants were significantly higher than the machine-turned implants ($P < 0.05$). The TiP-3 implants showed the highest mean RTV among investigated groups, significantly higher than the TiP-1 implants ($P < 0.05$). The mean RTV of the TiP-3 implants was higher than the TiP-2 implants, but was not statistically different ($P = 0.107$).

4. Discussion

In this study, we investigated the surface characteristics, osteoblastic cell response and biomechanical anchorage of P-incorporated Ti oxide surfaces produced by hydrothermal treatment using various concentrations of H_3PO_4. High concentrations of H_3PO_4 treatment produced more homogenous crystalline P-incorporated oxide layers with micro-rough surface topographies (TiP-2 and TiP-3), whose surfaces had superior wettabilities than untreated machined or Ti surfaces treated with lower H_3PO_4 concentrations (TiP-1). The chemical composition and Ti/P molar ratio (1.05) of the TiP-3 surface were quite close to that expected for $Ti_2O(PO_4)_2(H_2O)_2$.

The P-incorporated surfaces showed better osteoblast responses, and significantly increased strength of the bony integration of implants, which was evaluated by removal torque forces, compared with untreated machine-turned implants. These results coincide with a previous in vivo study showing improved osseoin-

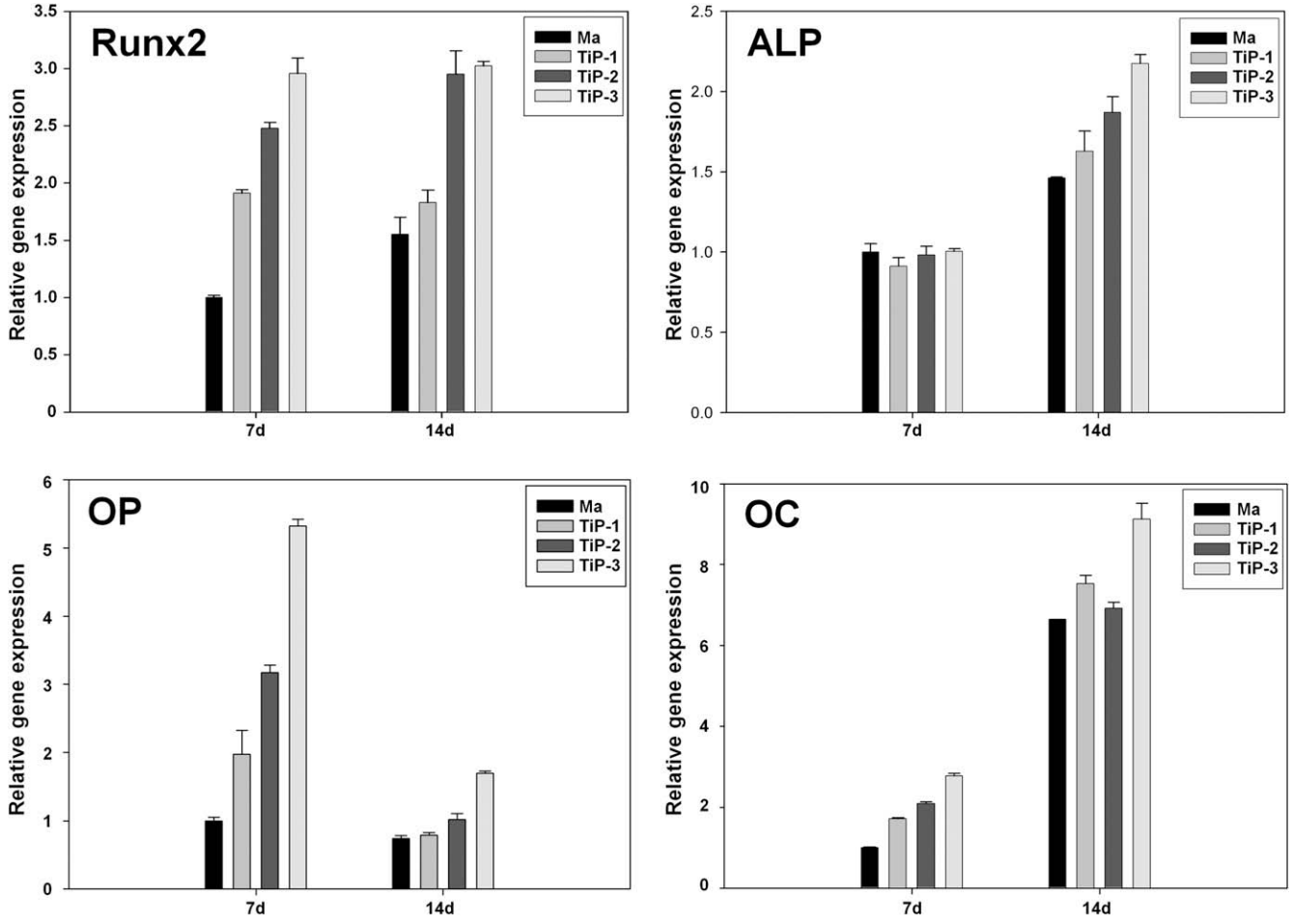

Fig. 8. Quantitative real-time PCR analysis of the levels of mRNA for Runx2, alkaline phosphatase (ALP), osteopontin (OP) and osteocalcin (OC) of MC3T3-E1 cells on different surfaces at 7 and 14 days of culture. Values are the mean ± SD of three independent measurements.

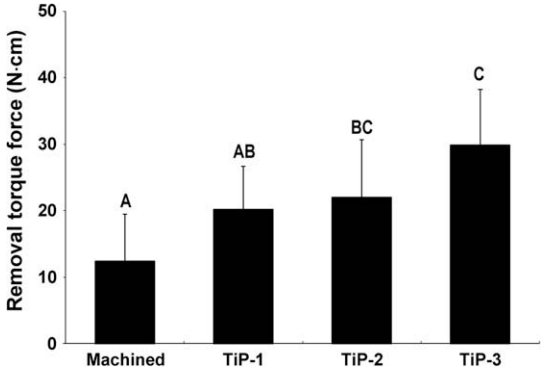

Fig. 9. Removal torque values (RTVs; N cm) of screw implants 4 weeks after implantation in rabbit tibiae. The RTVs for machined, TiP-1, TiP-2 and TiP-3 implants were 12.4 ± 7.1, 20.2 ± 6.5, 22.0 ± 8.7 and 29.9 ± 8.3 N cm, respectively. Data are reported as the mean ± SD (n = 7 per group). $^{A–C}$Values indicated by the same letters are not significantly different by Tukey's multiple comparison at α = 0.05.

tegration with P-incorporated Ti oxide surfaces compared with various commercial microstructured surfaces in rabbit tibiae [9].

Enhanced initial cell attachment and spreading on P-incorporated micro-rough surfaces are in agreement with the results of other studies reporting better adhesion and spreading of osteoblastic cells on grit-blasted or grit-blasted/etched micro-rough surfaces compared with relatively smooth machined surfaces [22–25]. However, in this study, Ti surfaces, which had almost identical R_a values (machined and TiP-1), showed different osteoblastic cell behaviors and removal torque forces. Thus, these results may not be fully explained by the roughness-dependent effects of the R_a value itself. Enhanced osteoblast attachment on TiP-1 surfaces compared with machined surfaces seemed to be attributed to better surface wettability. Numerous studies have suggested that more hydrophilic surfaces enhance osteoblast adhesion in vitro [26,27], which show more rapid bone apposition than hydrophobic surfaces in vivo [9–11]. Studies have indicated the increased adsorption of cell-adhesion-promoting extracellular matrix proteins on such wettable surfaces as a possible reason for the enhanced biocompatibility of those surfaces [26,27]. In this study, the surface hydrophilicity of Ti surface was increased by increasing the P content. Among the P-incorporated Ti surfaces, the TiP-2 and TiP-3 surfaces, which had higher P contents, showed significantly increased surface hydrophilicity compared with the TiP-1 surfaces with lower P contents. It appears that a homogenous Ti oxide layer with phosphate hydrate chemistry covering the surfaces may contribute to better wettability.

MC3T3-E1 cells grown on the P-incorporated surfaces showed notably higher expressions of key osteoblast genes – a major transcription factor regulating the osteoblast differentiation (Runx2 [28,29]), the early markers (ALP [30], osteopontin [31]) and the later marker (osteocalcin [32,33]) for osteoblast differentiation – than those grown on the machined surfaces. The expression of the osteoblastic phenotype genes paralleled a similar induction

to Runx2, with the exception of ALP expression at 7 days, and the levels of osteopontin expression at 7 days paralleled the amounts of P content in the surfaces and the released P ions from the P-incorporated surfaces. Recent studies demonstrated the role of phosphate during osteoblast differentiation; the active phosphate-transporting ability of cells was suggested as a requirement for the bone mineralization process [34–37]. Elevated free phosphate levels in the culture medium upregulated osteopontin gene expression and mineralization in MC3T3-E1 cells [34–37]. The results of notably increased expressions of osteopontin mRNA on P-incorporated surfaces at 7 days are in agreement with those studies reporting phosphate as a specific signal for the induction of the osteopontin gene expression. ICP-MS analysis showed more P ions released from Ti surfaces with higher P contents. The increase in P released from TiP-3 surfaces seems to be attributed to an increased surface area compared with TiP-2 surfaces with similar R_a values.

The degree of biomechanical anchorage of P-incorporated implants with bone tissue, which was evaluated by removal torque testing, showed tendencies to increase compared with untreated machine-turned implants. P-incorporated implants showed a 1.6- to 2.4-fold increase in mean removal torque values (RTVs) compared with machine-turned implants, indicating strong bone attachment behavior of P-incorporated surfaces. Ti implants treated using 2% (w/w) phosphoric acid showed higher mean RTV than those treated using lower concentrations of phosphoric acid (0.5% or 1%) and machine-turned implants. Removal torque testing has been used as a valuable biomechanical method to evaluate the strength of implant integration in bone tissue [17–20]. Higher RTVs may indicate an increased implant stability to withstand functional loads in the bone tissue. Micro-rough surface properties, including roughness, were correlated with enhanced implant stability by achieving micromechanical interlocking with bone tissue [18,20]. The machined and TiP-1 implants had almost identical minimally rough R_a values, but the TiP-1 implants showed a higher mean RTV than the machined implants. We suppose that P chemistry and superior wettability contributed to this result, which may indicate strong bone integration ability caused by possible biochemical bone bonding behavior of P-incorporated surfaces [5,6,9].

Between the Ti surfaces having similar moderately micro-rough R_a values and wettability (TiP-2 and TiP-3 surfaces), the TiP-3 surfaces showed increased tendencies in the expression of osteoblastic genes and RTV compared with the TiP-2 surfaces. It seems that these results are attributed to a larger surface area developed by the TiP-3 surfaces (by 157%) than that of the TiP-2 surfaces (by 65%). We suppose that larger surface area of the TiP-3 surfaces further contributed to higher RTV by achieving stronger micromechanical interlocking with bone tissue compared with the TiP-1 and TiP-2 surfaces.

Ti surfaces with a more homogenously covered P-incorporated oxide layer (TiP-2) showed significantly increased wettability compared with those with a nonhomogenous P-incorporated oxide layer (TiP-1), but no difference was found in RTVs between the two groups, despite different wettabilities and R_a values, although the surfaces showed some differences in the levels of osteoblastic gene expression. We need further detailed studies on this, including histomorphometric studies, to investigate if there are differences in the degree of bone apposition between these surfaces.

In this study, P-incorporated Ti oxide surfaces significantly enhanced cell attachment, osteoblastic gene expression and removal torque forces compared with machined surfaces. The primary mechanisms of action of enhanced osteoblastic cell behaviors and biomechanical anchorages are likely to be by surface wettability and P chemistry. Superior wettability might promote integrin-mediated cell attachment by increasing the adsorption of cell attachment-promoting proteins, and P might play an important role as a specific signal for inducing osteoblast cell differentiation. In addition, moderately micro-rough surface features and an increased surface area may be beneficial to further enhance osteoblast differentiation and biomechanical anchorages of P-incorporated surfaces [9,12,18,20]. Thus, we suggest that more micro-rough surface features, an increased surface area and abundant P contents might be more suitable for achieving more favorable bone healing of this type of P-incorporated Ti implant.

5. Conclusions

In this study, hydrothermal treatment using various concentrations of H_3PO_4 produced Ti surfaces with different surface characteristics. The P-incorporated Ti surfaces showed enhanced osteoblast attachment, osteoblast gene expression and removal torque forces compared with untreated machined surfaces. High concentrations of H_3PO_4 treatment produced more micro-rough and better wettable surfaces, and these surfaces also showed better osteoblastic cell responses and increased biomechanical anchorage. The results indicate that the various P-incorporated Ti oxide surfaces produced by hydrothermal treatment with H_3PO_4 may be an effective approach for enhancing implant osseointegration by stimulating osteoblastic cell attachment and differentiation on their surfaces and by achieving stronger bone–implant fixation.

Acknowledgements

This research was supported by Basic Science Research Program through the National Research Foundation of Korea (NRF) funded by the Ministry of Education, Science and Technology (No. R13-2008-009-01001-0). The authors thank Mr Jeong-Yoon Ha, Graduate School of Dentistry, Kyungpook National University, for his assistance with Fig. 4.

References

[1] Cooper LF, Zhou Y, Takebe J, Guo J, Abron A, Holmen A, et al. Fluoride modification effects on osteoblast behavior and bone formation at TiO_2 grit-blasted c.p. titanium endosseous implants. Biomaterials 2006;27:926–36.
[2] Guo J, Padilla RJ, Ambrose W, de Kok IJ, Cooper LF. The effect of hydrofluoric acid treatment of TiO_2 grit blasted titanium implants on adherent osteoblast gene expression in vitro and in vivo. Biomaterials 2007;28:5418–25.
[3] Park JW, Park KB, Suh JY. Effects of calcium ion incorporation on bone healing of Ti6Al4V alloy implants in rabbit tibiae. Biomaterials 2007;28:3306–13.
[4] Park JW, Suh JY, Chung HJ. Effects of calcium ion incorporation on osteoblast gene expression in MC3T3-E1 cells cultured on microstructured titanium surfaces. J Biomed Mater Res A 2008;86:116–7.
[5] Sul YT. The significance of the surface properties of oxidized titanium to the bone response: special emphasis on potential biochemical bonding of oxidized titanium implant. Biomaterials 2003;24:3893–907.
[6] Sul YT, Johansson C, Byon E, Albrektsson T. The bone response of oxidized bioactive and non-bioactive titanium implants. Biomaterials 2005;26:6720–30.
[7] Sul YT, Johansson CB, Jeong Y, Albrektsson T. The electrochemical oxide growth behaviour on titanium in acid alkaline electrolytes. Med Eng Phys 2001;23:329–46.
[8] Wang XX, Yan W, Hayakawa S, Tsuru K, Osaka A. Apatite deposition on thermally and anodically oxidized titanium surfaces in a simulated body fluid. Biomaterials 2003;24:4631–7.
[9] Park JW, Jang JH, Lee CS, Hanawa T. Osteoconductivity of hydrophilic microstructured titanium implants with phosphate ion chemistry. Acta Biomater 2009;5:2311–21.
[10] Buser D, Broggini N, Wieland M, Schenk RK, Denzer AJ, Cochran DL, et al. Enhanced bone apposition to a chemically modified SLA titanium surface. J Dent Res 2004;83:529–33.
[11] Eriksson C, Nygren H, Ohlson K. Implantation of hydrophilic and hydrophobic titanium discs in rat tibia: cellular reactions on the surfaces during the first 3 weeks in bone. Biomaterials 2004;25:4759–66.
[12] Schneider GB, Zaharias R, Seabold D, Keller J, Stanford C. Differentiation of preosteoblasts is affected by implant surface microtopographies. J Biomed Mater Res A 2004;69:462–8.
[13] Trisi P, Lazzara R, Rao W, Rebaudi A. Bone-implant contact and bone quality: evaluation of expected and actual bone contact on machined and osseotite implant surfaces. Int J Periodontics Restorative Dent 2002;22:535–45.

[14] Zhao G, Schwartz Z, Wieland M, Rupp F, Geis-Gerstorfer J, Cochran DL, et al. High surface energy enhances cell response to titanium substrate microstructure. J Biomed Mater Res A 2005;74:49–58.
[15] Park JW. Method of fabricating implant with improved surface properties and implant fabricated by the same method. KR Patent No. 100775537; 2007.
[16] Ishiyama M, Miyazono Y, Sasamoto K, Ohkura Y, Ueno K. A highly water-soluble disulfonated tetrazolium salt as a chondrogenic indications for NADH as well as cell viability. Talanta 1997;44:1299–305.
[17] Johansson CB, Han CH, Wennerberg A, Albrektsson T. A quantitative comparison of machined commercially pure titanium and titanium–aluminum–vanadium implants in rabbit bone. Int J Oral Maxillofac Implants 1998;13:315–21.
[18] Klokkevold PR, Johnson P, Dadgostari S, Caputo A, Davies JE, Nishimura RD. Early endosseous integration enhanced by dual acid etching of titanium: a torque removal study in the rabbit. Clin Oral Implants Res 2001;12:350–7.
[19] Sul YT, Kang BS, Johansson C, Um HS, Park CJ, Albrektsson T. The roles of surface chemistry and topography in the strength and rate of osseointegration of titanium implants in bone. J Biomed Mater Res A 2009;89:942–50.
[20] Szmukler-Moncler S, Perrin D, Ahossi V, Magnin G, Bernard JP. Biological properties of acid etched titanium surface. Effect of sandblasting on bone anchorage. J Biomed Mater Res B Appl Biomater 2004;68:149–59.
[21] Zhu X, Chen J, Scheideler L, Reichl R, Geis-Gerstorfer J. Effects of topography and composition of titanium surface oxides on osteoblast responses. Biomaterials 2004;25:4087–103.
[22] Keller JC, Schneider GB, Stanford CM, Kellogg B. Effects of implant microtopography on osteoblast cell attachment. Implant Dent 2003;12:175–81.
[23] Sammons RL, Lumbikanonda N, Gross M, Cantzler P. Comparison of osteoblast spreading on microstructured dental implant surfaces and cell behaviour in an explant model of osseointegration. Clin Oral Implants Res 2005;16:657–66.
[24] Zhao G, Zinger O, Schwartz Z, Wieland M, Landolt D, Boyan BD. Osteoblast-like cells are sensitive to submicron-scale surface structure. Clin Oral Implants Res 2006;17:258–64.
[25] Zhao G, Raines AL, Wieland M, Schwartz Z, Boyan BD. Requirement for both micron- and submicron scale structure for synergistic responses of osteoblasts to substrate surface energy and topography. Biomaterials 2007;28:2821–9.
[26] Shibata Y, Hosaka M, Kawai H, Miyazaki T. Glow discharge plasma treatment to titanium plates enhances adhesion of osteoblast-like cells to the plates through the integrin-mediated mechanism. Int J Oral Maxillofac Implants 2002;17:771–7.
[27] Yamamoto H, Shibata Y, Miyazaki T. Anode glow discharge plasma treatment of titanium plates facilitates adsorption of extracellular matrix proteins to the plates. J Dent Res 2005;84:668–71.
[28] Komori T. Regulation of skeletal development by the Runx family of transcription factors. J Cell Biochem 2005;95:445–53.
[29] Komori T. Regulation of osteoblast differentiation by transcription factors. J Cell Biochem 2006;99:1233–9.
[30] Aubin JE. Advances in the osteoblast lineage. Biochem Cell Biol 1998;76:899–910.
[31] Robey PG, Boskey AL. The biochemistry of bone. In: Marcus R, Feldman D, Kelsey J, editors. Osteoporosis. San Diego, CA: Academic Press; 1996. p. 95–183.
[32] Boskey AL, Gadaleta S, Gundberg C, Doty SB, Ducy P, Karsenty G. Fourier transform infrared microspectroscopic analysis of bones of osteocalcin-deficient mice provides insight into the function of osteocalcin. Bone 1998;23:187–96.
[33] Ducy P, Karsenty G. Genetic control of cell differentiation in the skeleton. Curr Opin Cell Biol 1998;10:614–9.
[34] Beck Jr GR, Zerler B, Moran E. Phosphate is a specific signal for induction of osteopontin gene expression. Proc Natl Acad Sci USA 2000;97:8352–7.
[35] Beck Jr GR. Inorganic phosphate as a signaling molecule in osteoblast differentiation. J Cell Biochem 2003;90:234–43.
[36] Kang HY, Shyr CR, Huang CK, Tsai MY, Orimo H, Lin PC, et al. Altered TNSALP expression and phosphate regulation contribute to reduced mineralization in mice lacking androgen receptor. Mol Cell Biol 2008;28:7354–67.
[37] Wu X, Itoh N, Taniguchi T, Nakanishi T, Tanaka K. Requirement of calcium and phosphate ions in expression of sodium-dependent vitamin C transporter 2 and osteopontin in MC3T3-E1 osteoblastic cells. Biochim Biophys Acta 2003;1641:65–70.